

Experimental assessment of a broadband vibration and acoustic emission sensor for rotorcraft transmission monitoring

Cristobal Ruiz-Carcel¹, Andrew Starr¹, and Arturo Francese¹

¹ *Cranfield University, Cranfield, Bedfordshire MK430AL, United Kingdom*

c.ruizcarcel@cranfield.ac.uk

a.starr@cranfield.ac.uk

a.francese@cranfield.ac.uk

ABSTRACT

Modern rotorcrafts rely on Health and Usage Monitoring Systems (HUMS) to enhance their availability, reliability, and safety. In those systems, data related to the health of key mechanical components is acquired, in addition to typical flight condition history data such as speed and torque. Commercial HUM systems usually rely on vibration measurements to assess the condition of shafts, gears, and bearings; using techniques such as spectral analysis, harmonic analysis, vibration trend and others. Recent research has shown that acoustic emissions (AE) can be advantageous in the detection of mechanical faults, in particular detecting very early small defects on bearings and gears, providing extra time for maintenance planning. However, the addition of extra sensors adds complexity and weight to the HUMS system, which is undesirable. This research is an experimental study to assess the monitoring capabilities of a broadband sensor, able to cover both low frequency vibration components as well as ultrasonic events, hence combining the benefits of both in a single compact sensing unit. The experimental results obtained from an instrumented rig using healthy components as well as seeded faults show the ability of the sensor to detect high frequency events, and compares the performance of the sensor in the low frequency range with a commercial accelerometer.

1. INTRODUCTION

Health and Usage Monitoring Systems (HUMS) are used to monitor rotorcraft power transmission systems, typically using predefined vibration features to assess their condition (Decker, 2002; Zakrajsek et al., 1993, 1995). HUMS was originally developed in North Sea operations, especially after the accident of a Boeing-Vertol 234 in 1986 caused by a main gearbox failure.

HUMS have two main functions, health monitoring and usage monitoring. The first aims to diagnose mechanical damage in the very early stages of degradation, before it leads to catastrophic damage. Usage monitoring focuses on the assessment of operation hours, current components condition and load history to estimate remaining life of mechanical components (Decker & Lewicki, 2003; Samuel & Pines, 2005). Commercial HUMS make use of different vibration analysis methods to detect faults in bearings, gears and shafts. Condition Indicators (CI's) are key vibration features extracted from the acquired vibration signals, which can be related to specific mechanical faults (Dempsey et al., 2008). In HUMS a range of different CI's are extracted from vibration data to characterize component health.

Vibration analysis has been traditionally grouped in three main categories; time domain, frequency domain and time-frequency domain. Time domain analysis pre-processes the raw signals (if necessary) and extracts features such as rms, skewness, and kurtosis (Martin, 1989; Sait & Sharaf-Eldeen, 2011). The Fast Fourier transform (FFT) is commonly used to obtain the frequency spectra of the signals, revealing their fundamental components. Fault detection in the frequency domain is based on identification of certain frequencies associated with bearing or gear faults. The amplitude of the components associated to those frequencies is then used as a CI. Time-frequency domain methods are able to track changes in the signal composition over time, including techniques such as short-time Fourier transform (STFT) (Mehala & Dahiya, 2008), Wigner-Ville (Sait & Sharaf-Eldeen, 2011), and wavelet analysis (Wang & McFadden, 2010).

Acoustic emissions (AE) in the field of machine monitoring are defined as transient elastic waves produced by the interface of two components or more in relative motion (Mba & Rao, 2006). Typical AE sources include impacts, crack growth, friction, turbulence, material loss, cavitation, leakage etc. Its main benefit against vibration analysis and oil analysis is the capability to detect faults earlier due to the high sensitivity offered by AE (Tan et al., 2007). On the other

Cristobal Ruiz-Carcel et al. This is an open-access article distributed under the terms of the Creative Commons Attribution 3.0 United States License, which permits unrestricted use, distribution, and reproduction in any medium, provided the original author and source are credited.

hand, the main drawback of AE is the difficulty in processing, interpreting and manipulating the acquired data (Al-Ghamd & Mba, 2006; Couturier & Mba, 2008). In addition, AE waves suffer a rapid attenuation of the signal, and require the AE sensor to be close to the source.

Vibration-based gearbox monitoring is well established, however the application of AE to this field is still in its early stages (Y. Qu et al., 2013; Tan et al., 2007) and it is difficult to see it implemented in commercial tools. In the area of HUMS some research has been carried out in recent years to prove the capabilities of AE to monitor helicopter transmission components, focusing on epicyclic gearboxes (Duan et al., 2015; Elasha et al., 2017; A. Qu et al., 2013). These investigations concluded that AE offered much earlier indication of damage than vibration analysis, and the proposed processing techniques were suitable for gearbox fault diagnosis.

Helicopter transmission systems are quite complex and compact, with difficult access and a requirement for lightweight. Hence it is necessary to simplify the monitoring system as much as possible, minimizing the number of sensors and wiring to reduce weight and requirements for sensor installation. The research in this paper assesses the capabilities of a broadband acoustic emission sensor, with a frequency range of 0.1 Hz to 1MHz, as a unique AE and vibration sensing unit for helicopter gearbox monitoring. Although the theoretical frequency range covered by the sensor supports its suitability as a vibration sensor as well as an AE sensor, in practice it is extremely difficult to build a sensor with a flat frequency response in such a wide range, which could hinder fault detection based on traditional vibration analysis. Consequently, the objective of this research is to compare the monitoring capabilities of this sensor with a commercial accelerometer, based on analysis of signals obtained on a laboratory scale rig where faults were artificially introduced. After signal amplification and digitation, the signal is high and low pass filtered to divide the AE and vibration content in it, which are analyzed separately. The main benefit of such approach is the simplification of the sensing unit, minimizing weight and required space, while maintaining the benefits of vibration and AE monitoring simultaneously.

2. METHODOLOGY

2.1. Sensing

The iMPactXS high-performance acoustic emission and dynamic load sensor manufactured by iNDTact GmbH was selected due to its frequency range (0.1 Hz to 1MHz) and sensitivity (> 1200 pC/N). As shown in Figure 1, this sensor covers the typical frequency ranges of both, vibration and AE sensors. The sensors were connected to an iNDTact champ charge amplifier, and the signals were digitized at 2 MHz

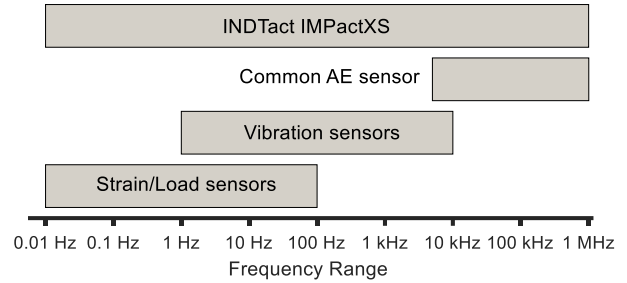


Figure 1: Typical frequency band of different sensors (iNDTact GmbH, 2022)

using a Pico Technology PicoScope 4224 IEPE digital oscilloscope.

Accelerometers are characterized by a flat frequency response in their usable frequency range, typically up to 10 or 20 kHz. That characteristic allows a direct conversion of the sensor output signal in mV to acceleration in ms^{-2} , as the sensitivity is constant in that limited frequency region. In order to assess the vibration monitoring capabilities of the broadband sensor, a commercial accelerometer will also be used simultaneously during the tests. A triaxial accelerometer (Brüel & Kjaer 4535-B) with a frequency range of 0.3 to 10000 Hz in the X and Y axes, and 0.3 to 12800 Hz in Z was selected. The voltage sensitivity is 1 mV/ ms^{-2} . Vibration signals were sampled at 51.2 kHz using a National Instruments 9234C data acquisition card.

In order to ensure that the transmission path for both sensors is equivalent a special sensor cluster was designed. Both sensors were installed in a compact machined aluminum block as shown in Figure 2. The AE sensor was glued using Dow Corning 3140 as a wave couplant, whereas the AE sensor was bolted to the metal block with an M3 stud. The cluster was attached to the rig using Loctite EA 9492.



Figure 2: Sensor cluster detail

2.2. Signal processing strategy

The signal processing strategy used for both sensors is represented in the diagram in Figure 3. Once digitized the vibration signals are processed directly for feature extraction. The AE signals however, after preamplification and digitation are divided in two categories using digital low and high pass filters with a cut-off frequency of 20 and 70 kHz respectively. Such approach allows for individual analysis of “low frequency” vibration-like events (such as oscillations

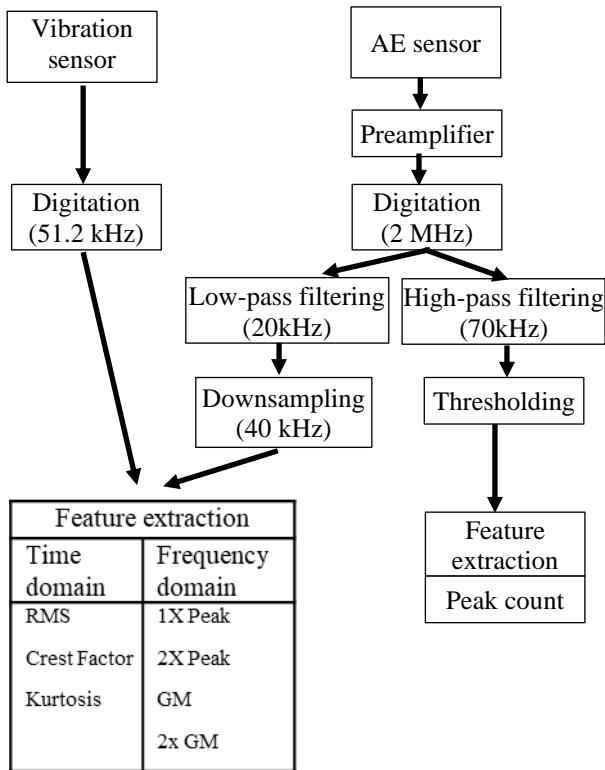


Figure 3: Data analysis workflow

related to misalignment, unbalance, gear mesh, bearing faults or resonances) independently from “high frequency” events such as impacts, friction or crack growth. The low frequency part of the signal is then down sampled to 40 kHz, which is enough to accurately represent the vibration signature and reduces computational cost. The features extracted from vibration signals in the time domain are RMS, crest factor and Kurtosis. The frequency spectrum is obtained using the FFT, and the peak amplitudes at the input shaft frequency (1X), the second harmonic (2X), the gear mesh frequency (GM) and its harmonic (2xGM) are extracted. This collection of CI’s is equal for both, the vibration sensor and the low frequency part of the broadband sensor. The selected CI’s are basic, well understood and widely used in gear monitoring, making them appropriate for this comparison exercise. The



Figure 4: Gearbox rig

high frequency part is analysed by setting a threshold above

the background noise level (thresholding), and counting the number of occasions the signal exceeded that threshold.

2.3. Experimental setup

The rig used to assess the performance of the sensors is a single stage gearbox rig (Figure 4), powered by an 11kW induction motor with 2 pairs of poles, and a nominal speed of 1490 rpm. The output shaft is connected to a dynamometer that absorbs and measures the load applied. The gear pair has straight teeth, a module of 5, and 24 and 25 teeth in the input and output shafts respectively. A lubrication port on the gearbox casing cover provided lubrication from an external pump. Although this benchtop arrangement is quite different from a helicopter gearbox in terms of shape, size, power, and stiffness, the gear meshing dynamics are the same as in any gear pair. The transmission path for the fault generated forces through the gears, shafts, and bearings to the static components are also comparable. Figure 5 (left) shows a detail of the gear pair. Figure 5 (right) shows the location of the sensor cluster, installed on a flat surface in the vicinity of the input shaft bearing housing.



Figure 5: Gear pair (left) and sensor cluster location (right)

In addition to the AE sensor and the triaxial accelerometer, the rig is equipped with a shaft speed sensor and a torque sensor. Temperature of the sensor cluster was also measured using a thermocouple.

2.4. Testing procedure

Data from both sensors, as well as speed, torque and temperature measurements were acquired during testing. The dynamometer was set to four different torque setpoints (10, 20, 30, and 40 Nm) to assess the sensor response at different loads. Vibration data was acquired in recordings of 1s, while the broadband sensor data recordings lasted 0.2s in order to keep a reasonable volume of data due to high sampling rate.

Initially the rig was operated with healthy gears to set a baseline for all the CI’s studied. Spalling was artificially introduced in the contact surface of one of tooth in the diver side gear to study the evolution of the CI’s. This failure mode was selected as planetary gear sets are more vulnerable to pitting defects due to intricate lubrication conditions. With the increase of the running cycles, the micro pitting will

induce more deleterious faults, such as spalling and chipping (Huangfu et al., 2022) Three different defect sizes were tested, drilling holes on the gear tooth surface of 0.8 (small), 1 (medium) and 1.5 (large) mm of diameter and around 0.2 mm in depth (Figure 6).



Figure 6: Detail of artificially introduced spalling

3. RESULTS AND DISCUSSION

3.1. Signals Overview

3.1.1. High frequency/AE

In first place the high-pass filtered broadband sensor signal was observed to assess the capabilities of the broadband sensor to detect small defects. Figure 7 shows a sample of the signals acquired for the healthy case (top) and the small fault (bottom) under 30 Nm of load. The healthy signal is composed basically by background noise, and there are no obvious bursts or peaks in the signal that indicate detection of AE related events. The faulty case however shows a series of bursts that clearly stand out of the carpet level. In addition, the distance between those bursts is around 40 ms, which is the time it takes for a full input shaft rotation to occur. That is the rate at which the induced fault enters the gear mesh.

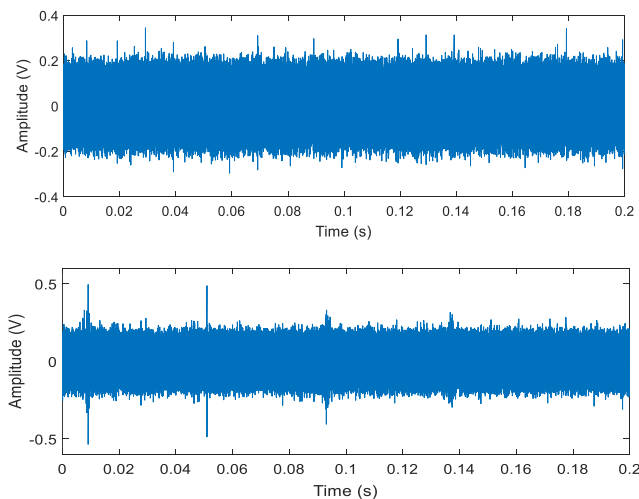


Figure 7: AE signal sample, healthy (top) and small fault (bottom) at 30 Nm

3.1.2. Low frequency/Vibration

For the comparison between the accelerometer and the low-frequency part of the broadband sensor, only the Z direction of the accelerometer (perpendicular to the mounting surface) was considered for simplicity, as it is the same direction the broadband sensor is measuring. Figure 8 shows an example of the frequency content from the signal acquired from both sensors in the healthy case and 30 Nm of load. It can be seen that despite the lack of faults the spectrum is dominated by the GM frequency and its harmonics, as usual in gearboxes. The spectrum also shows that these main peaks are surrounded by sidebands, spaced around 24 Hz (the input shaft frequency) from each other. That may be an indication that the alignment between the shafts is not perfect, and the gear mesh is being modulated in amplitude once per revolution.

When comparing the spectrum of both sensors, it can be seen that the frequency content of the broadband sensors is similar to the accelerometer, but the relative amplitude of the peaks differs. It is important to note that the units have been kept in V for both sensors and each one has its own scale, as the potential lack of linearity in the response of the broadband sensor does not allow a direct conversion to acceleration units. The results at the top graph in Figure 8 show that the broadband sensor is able to capture the most relevant components, GM and harmonics, but fails to accurately

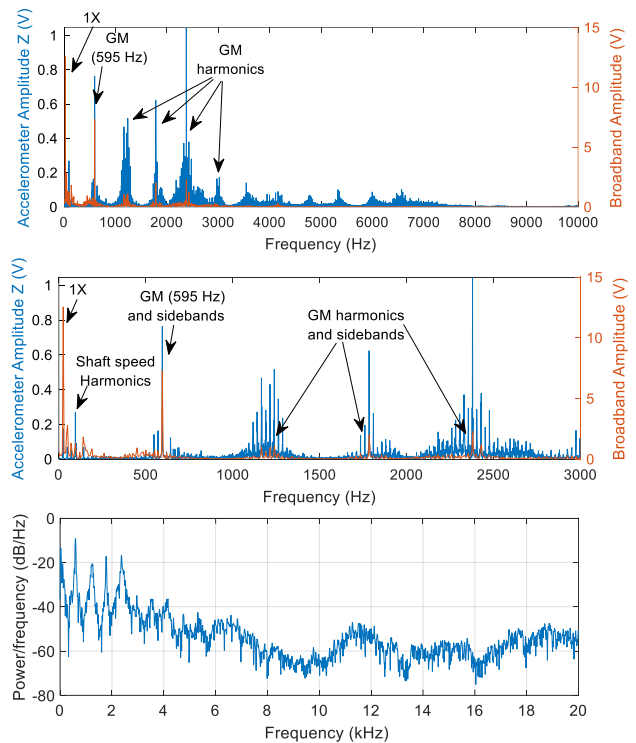


Figure 8: Frequency spectrum of accelerometer and broadband sensor signals up to 10 kHz (top), low frequency detail (centre) and Welch cross power spectral density estimate (bottom)

Table 1: Number of samples obtained in each case

Case	Healthy				Small				Medium				Large			
Torque (Nm)	10	20	30	40	10	20	30	40	10	20	30	40	10	20	30	40
Sample number	189	165	184	177	72	59	82	65	92	73	95	73	123	127	119	117

capture the amplitude of signal components beyond 3000 Hz. This observation is also corroborated by the Welch cross power spectral density estimate presented in Figure 8 (bottom). This analysis shows the highest coherence between the signals is found below 3 kHz and is particularly high for the GM frequency and its first harmonics. For higher frequencies the coherence is much lower. In principle that is not a huge problem, as the most typical vibration signatures in rotating machinery (shaft speed, GM, bearing defect frequencies, etc. and harmonics of all of them) typically happen in that region. However other important vibration phenomena, particularly resonances, typically happen between 3 and 10 kHz, which could be a problem for this sensor. On the other hand, the AE capabilities should be able to capture impact-like events even earlier than an accelerometer could detect a change in the amplitude of a resonant frequency.

The lack of linearity in the frequency response compared with the accelerometer is quite evident when looking closely at the amplitudes of the main components (Figure 8 centre). Even if the 1X peak amplitude and most of its harmonics are larger than the same peaks in the accelerometer signal spectrum with the selected axes ranges, the correlation is not maintained for higher frequency components (mainly GM, harmonics and sidebands). It can be concluded that the broadband sensor is not as good at responding linearly to a range of different frequencies as the accelerometer. This would be a problem for approaches where it is required to obtain an accurate measurement of acceleration at different frequencies. Commonly that is not the case in monitoring applications, where the typical procedure is to compare newly acquired measurements with a established baseline. From that perspective, repeatability and precision in the representation of amplitude for different frequency components are way more important than accuracy. As it will be seen later, repeatability in measured peak amplitudes was not an issue for this sensor. Despite the lack of fidelity in amplitude compared with the accelerometer, the broadband sensor was able to accurately identify the main frequency components in the signal, which is key to identify the sources of vibration and possible links to mechanical faults. Consequently, the signals acquired from the sensor are in principle adequate and acceptable for monitoring purposes. The next subsection will investigate fault detection performance.

3.2. Fault detection

Table 1 shows the number of samples obtained for each combination of torque and healthy/faulty case. The results will be presented displaying the average value of the CI

obtained for each combination, and the standard deviation of each sample will be represented in the form of an error bar around the mean value.

3.2.1. High frequency/AE

Presence of peaks in the AE signals for the healthy case should not happen, as only events related to faults produce AE activity. For the faulty cases peak count will depend on rotational speed, defect frequency and whether the amplitude of the AE generate is large enough to cross the threshold. Preliminary analysis of the AE signals obtained under healthy conditions, revealed that the maximum absolute value observed was on average 0.27 V (seen example in Figure 7 top). Consequently the threshold value above that carpet level was set to 0.3 V, which provided the peak counting results shown in Figure 9. As it can be seen, the number of threshold crossings found in the healthy case is small for all loads, and can be attributed to outliers slightly above the threshold level, which was chosen relatively low to enhance sensitivity. The effect of the fault was evident even in the small fault case, particularly for high loads. This result highlights the main benefit of AE and its capability to identify faults in the early stages of degradation. The medium and large fault cases also show larger number of threshold crossings than the healthy case, and the standard deviation in the samples is greater particularly in the large case.

3.2.2. Low frequency/Vibration

Figure 10 shows the results obtained from the time domain vibration CI's extracted from the accelerometer and the broadband sensor. RMS shows little sensitivity to the fault in the small and medium cases, and it was only in the large case that an increment in this indicator was obvious. The case of the CF is not very informative, as the changes in the mean values observed are in the same order of magnitude as the standard deviations. No significant differences with the healthy case are observed. Important to note that the CF is

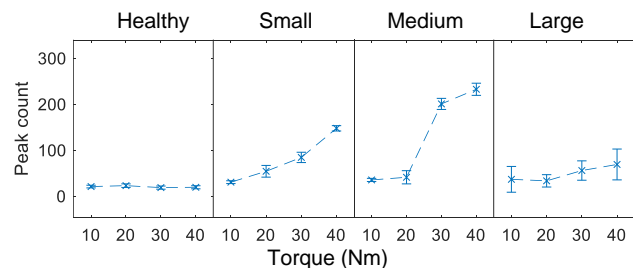


Figure 9: Average value and standard deviation for peak count from AE signal

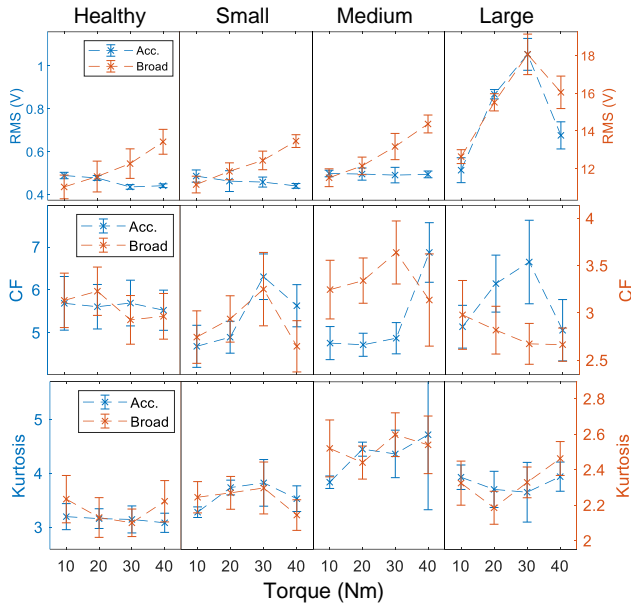


Figure 10: Average value and standard deviation for time domain CI's

typically twice as large for the accelerometer than for the broadband sensor, evidencing a larger signal to noise ratio. Kurtosis does not show any evident failure indications for the small case, but the values in the medium case are significantly larger than the healthy case, although they decay again for the large fault case. K values are smaller for the broadband sensor, pointing at a lack of “peakiness” in the signals compared with the accelerometer. It is important to note that despite the differences in magnitude between both sensors for all three indicators, their response to changes in load and presence of faults is similar.

The results obtained from frequency domain CI's are presented in Figure 11. The amplitude of the shaft speed peak (1X) shows no significant change with the small fault compared with the healthy case. However in both the medium and large cases there is an increment in the CI in both sensors, which is also appreciable as the load increases. The second harmonic of the shaft speed does not present significant changes in the presence of faults for any of the sensors, and any variations are in the same order of magnitude as the standard deviation for the healthy case. The GM peak amplitude shows a small increment for the medium and large faults, but not noticeable increments for the small fault. This CI is clearly correlated with load as well. Its second harmonic shows a very similar behaviour to the 2X case with even greater variability in the accelerometer measurements in the faulty cases. The broadband sensor shows some increment with respect to the healthy case in the medium and large fault cases, but again variability in this CI is too large to consider the differences significant.

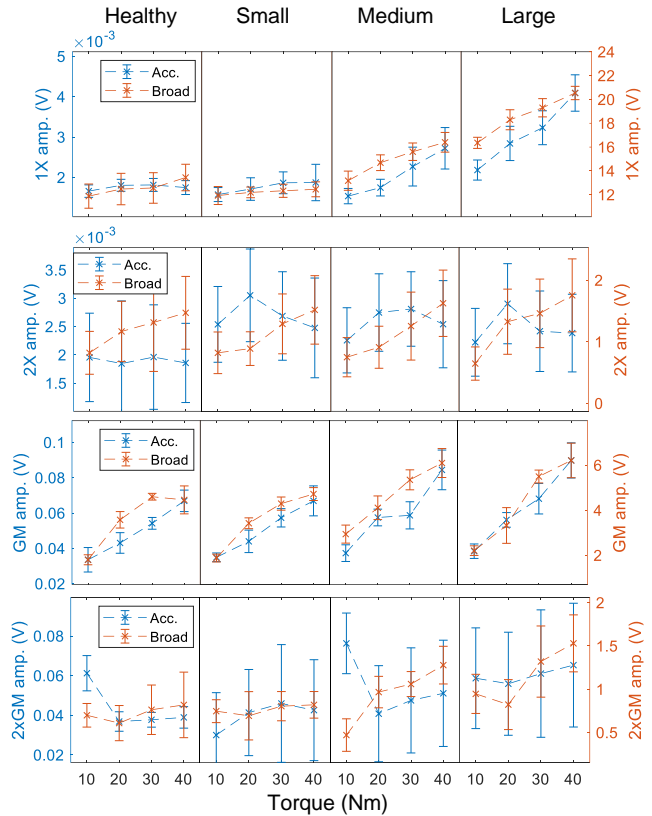


Figure 11: Average value and standard deviation for frequency domain CI's

Table 2 summarises the results presented in a tabular format, displaying the percentage change with respect to the healthy case of every CI considered in both sensors. It is quite clear that AE based peak counting was the only indicator providing a clear increment for the small fault case, as seen before the 2X peak amplitude measurements in the accelerometer had large variability and hence low significance. The 1X and GM peak amplitudes, together with Kurtosis were able to react to the medium and large cases. RMS was only sensitive to the large fault. Those results are quite consistent for both sensors.

4. CONCLUSION

The research presented in this paper focuses on an experimental validation of a broadband sensor for rotorcraft transmission monitoring, which combines AE and vibration monitoring capabilities in a single sensor. The validation was performed through comparison of the selected sensor with a conventional accelerometer, which were both tested on a dedicated gear rig operated at different loads where gear spalling at 3 different degradation stages was introduced artificially. The proposed data processing technique separates the broadband sensor signal in its low and high frequency regions, allowing the use of traditional vibration and AE analysis techniques to be applied for feature extraction.

Table 2: Mean value percent change with respect to the corresponding healthy case

Case	Large				Medium				Small			
	10	20	30	40	10	20	30	40	10	20	30	40
Torque												
RMS acc.	-0.5	-3.1	5.2	-0.2	1.9	3.8	12.7	12.0	5.1	82.1	142.6	53.5
RMS broad.	1.1	2.4	1.4	0.3	4.4	4.9	7.4	7.0	14.6	33.9	47.2	19.5
CF acc.	-17.6	-12.7	10.8	1.9	-16.3	-15.8	-14.4	24.4	-9.6	9.6	16.8	-8.4
CF broad.	-12.4	-9.1	11.1	-10.7	3.6	3.5	24.3	5.8	-4.9	-12.7	-8.7	-10.1
K acc.	2.6	8.8	2.5	1.5	20.0	40.8	38.7	53.0	22.9	17.2	16.0	27.8
K broad.	0.5	6.5	9.3	-3.5	12.8	14.5	23.6	14.3	4.0	2.6	10.8	10.8
1X acc.	-5.1	-5.1	2.9	7.2	-7.4	-3.2	25.0	55.6	31.4	57.4	78.0	133.8
1X broad.	0.4	-2.2	-1.9	-7.4	10.9	17.7	24.2	22.0	37.6	46.6	53.6	52.8
2X acc.	29.8	65.3	37.0	33.3	15.4	48.8	43.3	36.8	13.6	57.3	23.3	28.4
2X broad.	0.1	-23.9	-1.8	3.2	-8.7	-22.0	-4.5	10.5	-21.2	13.5	11.2	19.3
GM acc.	4.2	2.1	5.8	0.0	11.2	33.4	8.4	26.2	14.5	30.3	25.7	34.2
GM broad.	4.2	-4.3	-6.6	5.8	63.1	14.9	16.3	36.6	22.5	-7.0	19.5	39.2
2xGM acc.	-50.9	12.2	21.8	9.3	24.6	10.7	25.9	31.1	-4.1	51.6	61.7	67.6
2xGM broad.	6.8	13.9	5.4	0.1	-32.6	58.8	38.8	56.0	35.3	35.1	72.9	86.7
AE Peak count	45.6	135.5	349.0	656.5	68.5	79.0	967.6	1091.4	74.8	45.3	197.2	254.0

The results obtained showed that the high frequency analysis of the signal was able to detect the smallest fault introduced, proving its capability to provide early fault detection as expected from an AE sensor. The analysis of the spectrum for the low frequency part of the signal showed that the broadband sensor can identify the same signal components measured by the accelerometer, which are related to the operating conditions, the machine's components geometry and their condition. However, the relative amplitudes of those components were different to the observations in the accelerometer, pointing to a lack of linearity in the frequency response of the sensor in the frequency range where vibration components are typically manifested. Even though, the main components were still easily identifiable, and the amplitude measured was repeatable throughout the tests, proving its ability to consistently provide a reliable comparison with a baseline value. The amplitude of all components over 3 kHz was clearly diminished, which can be a problem for approaches that require the study of frequencies in this range, such as resonances.

The CI's extracted from both sensors showed a very similar response to changes in load and presence of faults, proving that the sensor is suitable for vibration monitoring based on analysis of basic vibration features. None of the vibration features studied provided a clear increment for the smallest fault studied that was statistically significant. For time domain analysis, RMS was only sensitive to the large fault, while Kurtosis showed some indication of change for the medium case. In frequency domain analysis, both the 1X and the GM CI's increased for the medium and particularly for the large case, proving effective in detecting the fault. Variability was too large in the analysis of CF, 2X and 2xGM. Future work will need to investigate if the similarities between the CI's from both sensors can be extended to more

complex vibration analysis techniques, such as bispectral analysis or cyclo-stationary analysis.

The most important conclusion from the analysis of this range of CI's was that the behaviour of both sensors was very similar (despite the differences in scale), proving that the capabilities of the broadband sensor for vibration-based monitoring are comparable to the accelerometer. Hence a monitoring system based solely on this sensor could combine the benefits of both, AE and vibration monitoring with a single sensing unit and combined data processing.

ACKNOWLEDGEMENT

This research has received funding from the Clean Sky 2 Joint Undertaking under the European Union's Horizon 2020 research and innovation programme under grant agreement No 738144.

REFERENCES

Al-Ghamd, A. M., & Mba, D. (2006). A comparative experimental study on the use of acoustic emission and vibration analysis for bearing defect identification and estimation of defect size. *Mechanical Systems and Signal Processing*, 20(7), 1537–1571. <https://doi.org/10.1016/j.ymssp.2004.10.013>

Couturier, J., & Mba, D. (2008). Operational bearing parameters and acoustic emission generation. *Journal of Vibration and Acoustics, Transactions of the ASME*, 130(2). <http://www.scopus.com/inward/record.url?eid=2-s2.0-45249088282&partnerID=40&md5=a193d74487821fb420a9e45cdfc1a6fd>

Decker, H. (2002). *Crack Detection for Aerospace Quality Spur Gears*. 15.

- Decker, H., & Lewicki, D. (2003). *Spiral Bevel Pinion Crack Detection in a Helicopter Gearbox*. 16.
- Dempsey, P., Keller, J., Wade, D., & Arsenal, R. (2008). *Signal Detection Theory Applied to Helicopter Transmission Diagnostic Thresholds*.
- Duan, F., Elasha, F., Greaves, M., & Mba, D. (2015). *Helicopter Main Gearbox Bearing Defect Identification using Vibration and Acoustic Emission Techniques*.
<https://doi.org/10.1109/ICPHM.2016.7542856>
- Elasha, F., Greaves, M., Mba, D., & Fang, D. (2017). A comparative study of the effectiveness of vibration and acoustic emission in diagnosing a defective bearing in a planetary gearbox. *Applied Acoustics*, 115, 181–195.
<https://doi.org/10.1016/J.APACoust.2016.07.026>
- Huangfu, Y., Dong, X., Chen, K., Tu, G., Long, X., & Peng, Z. (2022). A tribo-dynamic based pitting evolution model of planetary gear sets: A topographical updating approach. *International Journal of Mechanical Sciences*, 220, 107157.
<https://doi.org/10.1016/J.IJMECSCI.2022.107157>
- iNDTact GmbH. (2022, March 25). *Datasheet iMPactXS*.
https://www.indtact.de/_files/Ugd/5a81ff_463278d4e34446fabca5b70adf13c592.Pdf
- Martin, H. (1989). Statistical Moment Analysis as a Means of Surface Damage Detection. *Proceedings of the International Modal Analysis Conference*.
- Mba, D., & Rao, R. B. K. N. (2006). Development of acoustic emission technology for condition monitoring and diagnosis of rotating machines: Bearings, pumps, gearboxes, engines, and rotating structures. *Shock and Vibration Digest*, 38(2), 3–16.
<http://www.scopus.com/inward/record.url?eid=2-s2.0-32944479589&partnerID=40&md5=16e5b54a47634aaca6788c18bb5fad9f>
- Mehala, N., & Dahiya, R. (2008). *A comparative study of FFT, STFT and wavelet techniques for induction machine fault diagnostic analysis*.
- Qu, A., Hecke, B., He, D., Yoon, J., Bechhoefer, E., & Zhu, J. (2013). Gearbox Fault Diagnostics using AE Sensors with Low Sampling Rate. *Journal of Acoustic Emission*, 31, 67–90.
- Qu, Y., Hecke, B., van, He, D., & Yoon, J. (2013). *Gearbox Fault Diagnostics using AE Sensors with Low Sampling Rate*. 31, 67–90.
- Sait, A., & Sharaf-Eldeen, Y. (2011). A Review of Gearbox Condition Monitoring Based on vibration Analysis Techniques Diagnostics and Prognostics. In *Conference Proceedings of the Society for Experimental Mechanics Series* (Vol. 5, pp. 307–324).
https://doi.org/10.1007/978-1-4419-9428-8_25
- Samuel, P., & Pines, D. (2005). A review of vibration-based techniques for helicopter transmission diagnostics. *Journal of Sound and Vibration*, 282, 475–508.
<https://doi.org/10.1016/j.jsv.2004.02.058>
- Tan, C. K., Irving, P., & Mba, D. (2007). A comparative experimental study on the diagnostic and prognostic capabilities of acoustics emission, vibration and spectrometric oil analysis for spur gears. *Mechanical Systems and Signal Processing*, 21(1), 208–233.
<https://doi.org/10.1016/J.YMSSP.2005.09.015>
- Wang, W. W., & McFadden, P. D. (2010). Application of wavelets to gearbox vibration signal for fault detection. *Journal of Sound and Vibration*, 192, 927–939.
<https://doi.org/10.1006/jsvi.1996.0226>
- Zakrajsek, J., Townsend, D., & Decker, H. (1993). *An Analysis of Gear Fault Detection Methods as Applied to Pitting Fatigue Failure Data*.
- Zakrajsek, J., Townsend, D., Lewicki, D., Decker, H., & Handschuh, R. (1995). *Transmission Diagnostic Research at NASA Lewis Research Center*. 14.

BIOGRAPHIES

Dr. Cristobal Ruiz-Carcel Cristobal received his degree in mechanical engineering in 2010 from Universidad Politecnica de Valencia (Spain), followed by an MSc Eng. degree in Design of Rotating Machines from Cranfield University in 2011. In 2014 he completed his PhD in the field of condition monitoring applied to large scale industrial systems at Cranfield University, which was part of the Marie Curie FP7 project “Energy-Smartops”. Cristobal's main research interests have been focused on signal processing algorithms, multivariate data analysis, condition monitoring and predictive maintenance. He is currently a Research Assistant at the Centre for Life-cycle Engineering and Management, where he works on the development, testing, and implementation of novel monitoring techniques for different applications.

Prof. Andrew Starr is head of the Centre for Life-cycle Engineering and Management (CLEM), a world-leading centre of excellence in maintenance and asset management for high value systems. The centre works in partnership with industry in research and education. Professor Starr read Mechanical Engineering at the University of Leeds, while sponsored by British Aerospace (Civil Aircraft), for which he was awarded first prize in the final year of his apprenticeship. He studied for his doctoral thesis in condition based maintenance for robotic production plant at the University of Manchester, sponsored by Ford and Wolfson Maintenance. He has held academic posts at the University of Huddersfield, the University of Manchester, and the University of Hertfordshire, as Head of the School of Aerospace, Automotive and Design Engineering. He has published over 150 technical papers from a wide range of collaborative projects with industry, helping to solve real problems and to devise innovative products and services.

Arturo Francese is a chartered engineer working as senior stress engineer at Cranfield Aerospace Solution ltd. He has more than 20 years of experience in the aerospace industry, mainly in the stress department and in support to production team. During his career, he has been a signatory holder for concessions and design changes to legacy products. Currently he is involved with Cranfield University by supporting research projects and taught students.